



Resistive switching characteristics of solution-processed TiO_x for next-generation non-volatile memory application; transparency, flexibility, and nano-scale memory feasibility

Seungjae Jung^a, Jaemin Kong^a, Sunghoon Song^a, Kwanghee Lee^{a,b,c}, Takhee Lee^{a,c}, Hyunsang Hwang^{a,c,*}, Sanghun Jeon^{d,*}

^a School of Materials Science and Engineering, Gwangju Institute of Science and Technology (GIST), Buk-gu, Gwangju-si 500-712, Republic of Korea

^b Heeger Center for Advanced Materials, Gwangju Institute of Science and Technology (GIST), Buk-gu, Gwangju-si 500-712, Republic of Korea

^c School of Nanobio Materials and Electronics, Gwangju Institute of Science and Technology (GIST), Buk-gu, Gwangju-si 500-712, Republic of Korea

^d Devices Laboratory, Samsung Advanced Institute of Technology, Yongin-si, Gyeonggi-do 446-712, Republic of Korea

ARTICLE INFO

Article history:

Available online 30 March 2011

Keywords:

Resistive switching
ReRAM
Titanium oxide
Solution-process
Sol-gel
Transparent
Flexible
Nano-scale
Via-hole

ABSTRACT

Solution-processed TiO_x layer was investigated as a candidate for next-generation resistive random access memory (ReRAM) application. TiO_x active layer was prepared by simple spin coating process of a titanium(IV) isopropoxide precursor using sol-gel chemistry. Through the introduction of indium-tin-oxide (ITO) coated glass and polyethersulfone (PES) substrates, transparent and flexible ReRAM devices were demonstrated, respectively. In addition, using scalable via-hole structure with nano-scale active area, the feasibility for high-density memory application was investigated. All ReRAM devices formed using various substrates exhibited good memory performance, such as stable dc I-V, ac endurance, and retention characteristics during maintaining their own unique functions accomplished by substrate properties.

© 2011 Elsevier B.V. All rights reserved.

1. Introduction

Recently, resistive random access memory (ReRAM) have been considered as one of the most promising candidate for next-generation non-volatile memory, due to their great scalability, low power consumption, and non-destructive readout [1,2]. Among them, TiO_2 -based ReRAM devices have attracted great interest because of relatively well-known operation mechanism and compatibility with complementary metal-oxide-semiconductor process as compared to ternary or quaternary oxides, such as doped SrZrO_3 , SrTiO_3 , $(\text{Sm}, \text{Ca})\text{MnO}_3$ / $(\text{La}, \text{Sr})\text{MnO}_3$, and $(\text{Pr}, \text{Ca})\text{MnO}_3$ [3–8]. Especially, many researchers have widely investigated ReRAM devices for transparent, flexible, low-cost, and light-weight memory application, using solution-processible TiO_x layer [9–11]. However, the electrical reliability characteristics of the devices were still remained as main problems to be solved [9–11]. More-

over, up to date, most of solution-processed ReRAM devices have been fabricated and tested their feasibility in micron-scale [9–12]. Taking into account reliable memory performance, high-density memory application as well as the confirmation of their intrinsic properties, not only memory reliability improvement but also feasibility test in nano-scale should be performed. In this study, we successfully demonstrated the solution-processed TiO_x -based ReRAM device with active area of $200 \times 200 \text{ nm}^2$ using via-hole structures, together with the feasibility test for the transparency/flexibility of the device using indium-tin-oxide (ITO) coated glass and polyethersulfone (PES) substrates.

2. Experiments

A TiO_x active layer was prepared according to the procedure described elsewhere [13,14]: Titanium(IV) isopropoxide ($\text{Ti}[\text{OCH}(\text{CH}_3)_2]_4$, Aldrich, 99.999%, 10 mL) was introduced as a precursor of the TiO_x sol-gel product. The precursor was mixed with 2-methoxyethanol ($\text{CH}_3\text{OCH}_2\text{CH}_2\text{OH}$, Aldrich, 99.9+%, 50 mL) and ethanolamine ($\text{H}_2\text{NCH}_2\text{CH}_2\text{OH}$, Aldrich, 99+%, 5 mL). Then, the mixed solution was heated up to 80°C for 2 h with stirring, followed by heating to 120°C for 1 h in argon ambient. Subsequently, the

* Corresponding authors Address: School of Materials Science and Engineering, Gwangju Institute of Science and Technology (GIST), Buk-gu, Gwangju-si 500-712, Republic of Korea (H.Hwang).

E-mail addresses: hwanghs@gist.ac.kr (H. Hwang), sanghun1.jeon@samsung.com (S. Jeon).

product was cooled down to 25 °C and diluted using isopropyl alcohol. For transparent ReRAM (TRRAM) and flexible ReRAM (FRRAM) device fabrication, ITO-coated glass was cleaned by successive wet cleaning through ultrasonication for 15 min each in DI water, acetone, and IPA. ITO-coated PES was cleaned by mechanical cleaning with detergent and only DI ultrasonication due to the weakness against cleaning chemicals. Further, both the substrates were dried in a vacuum oven at 80 °C for 30 min, followed by UV/O₃ surface treatment. The TiO_x precursor solution was spin-coated directly on both the substrates and then hydrolyzed at room temperature for 1 h in air (TiO_x ~ 50 nm). Finally, an Al top electrode with an area of 50 × 50 μm² was formed by shadow mask and post-annealing was conducted at 150 °C in N₂ ambient.

Additionally, for nano-scale ReRAM device formed using via-hole structure, W/Ti/SiO₂/Si substrate was cleaned by the same process with that of ITO-coated glass. A 100 nm-thick SiO₂ was grown by plasma-enhanced chemical vapor deposition. Conventional lithography technique and reactive ion etching process were implemented to define nano-scale via-holes with area ranging from 50 × 50 μm² to 200 × 200 nm². Subsequent process for ReRAM device fabrication was followed by aforementioned process.

3. Results and discussions

Fig. 1a exhibits the absorption characteristic of TiO_x spin-coated on fused silica. From the absorption result, the prepared TiO_x film is completely transparent in the visible range from 400 to 700 nm (see also starting solution in the inset of Fig. 1b). Since entire fabrication process of our devices was below 150 °C, which is much lower than the crystallization temperature, complete amorphous TiO_x film was confirmed by X-ray diffraction analysis (Fig. 1b). Fig. 2 shows X-ray photoelectron spectroscopy (XPS) Ti 2p spectra of almost stoichiometric TiO₂ at surface (top) and oxygen-deficient TiO_x in the bulk (bottom). The XPS analysis was conducted in TiO_x film annealed at 150 °C to evaluate Ti chemical state in the complete device structure. Because the surface of prepared film was directly exposed to air, subsequent oxidation can be occurred during post-annealing. On the other hand, TiO_x in the bulk can be protected from additional oxidation. As expected, Ti 2p spectrum at the surface shows almost stoichiometric TiO₂-related peak (Ti⁴⁺ binding energy = 459.0 eV), while that in the bulk represents oxygen-deficient TiO_x-related peaks, resolving into Ti⁴⁺ and Ti³⁺ (binding energy = 457.6 eV) [15]. This result indicates that the prepared TiO_x film has oxygen vacancies, which is favorable for resistive switching properties of TiO_x [4]. Typically, TiO₂ films grown by

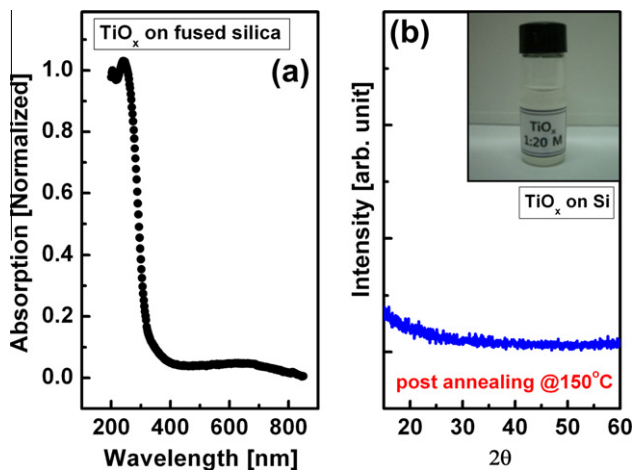


Fig. 1. (a) Optical absorption spectrum and (b) XRD pattern of solution-processed TiO_x film. The picture of starting TiO_x solution was also shown in the inset of (b).

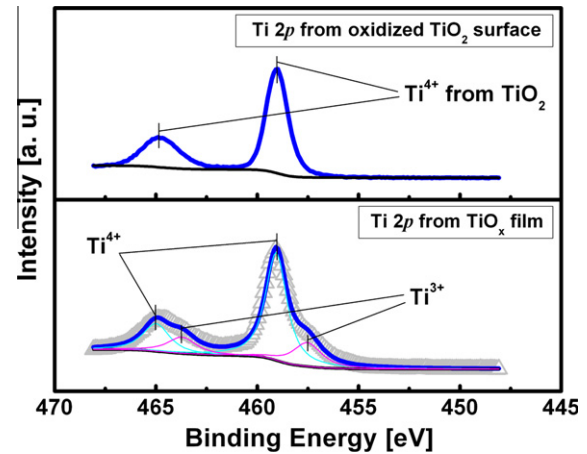


Fig. 2. Ti 2p portion of the XPS spectra of almost stoichiometric TiO₂ at surface and oxygen-deficient TiO_x in the bulk. The peaks of Ti 2p_{1/2} and Ti 2p_{3/2} were measured after post-annealing in nitrogen ambient at 150 °C.

vacuum process such as atomic-layer deposition, metal organic chemical vapor deposition, and reactive sputtering tend to include less oxygen vacancies, compared to solution-processed one [3–4,11,13,14,16–19]. This property is originated from the removal of organic element in starting solution after finishing hydrolysis reaction. This possibly helps the fast switching speed and low-voltage operation of the ReRAM device, but could lead to poor uniformity due to uncontrollable defect density and distribution. Study on the resistive switching characteristics depending on defect control based on sol-gel chemistry would be a valuable further study.

Fig. 3 shows the current–voltage (I–V) characteristics of our ReRAM device. During all the electrical measurement, an external bias was applied to the Al top electrode, and the ITO bottom electrode was electrically grounded. After initial forming process on positive side, the device exhibits stable bipolar switching behavior between low resistance state (LRS) and high resistance state (HRS) under consecutive dc voltage sweep of ±2 V up to 1000th cycle. In order to understand the resistive switching mechanism of solution-processed TiO_x, the log I–log V plot was evaluated, as shown in Fig. 4a. In LRS, the slope of the log I–log V plot is ~1.0, implying ohmic conduction. The conduction behavior in HRS at the low voltage region (<0.5 V) also can be explained by ohmic conduction. In contrast, in HRS at the high voltage region (>0.5 V), the slope of

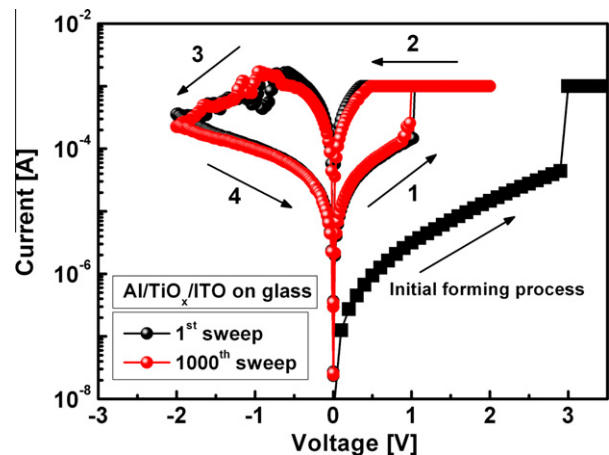


Fig. 3. Typical dc I–V characteristics up to 1000th sweep of solution-processed TiO₂-based ReRAM device. The initial forming process is also represented.

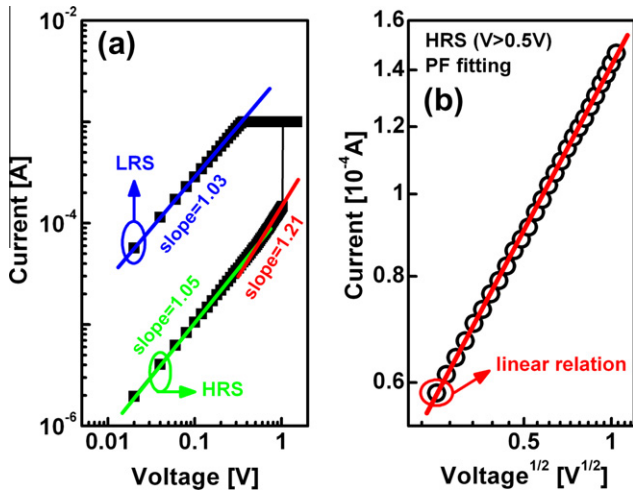


Fig. 4. (a) The log I to log V plot of solution-processed TiO₂-based ReRAM device. (b) The PF emission fitting of HRS at high voltage region (>0.5 V).

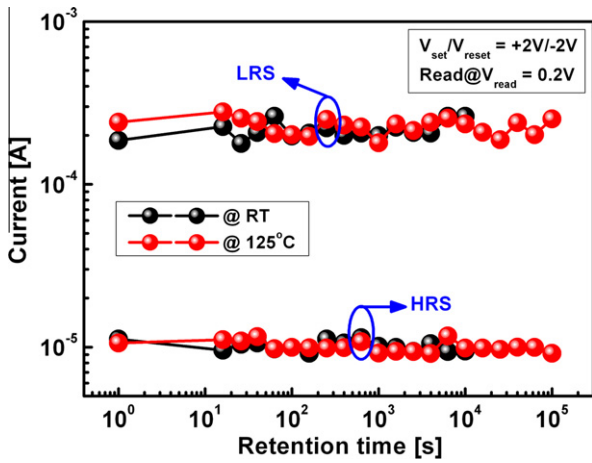


Fig. 5. Retention characteristics of solution-processed TiO₂-based ReRAM device at high temperature at 125 °C. Negligible fluctuation was observed up to 10⁵ s.

the fitted line increases up to 1.21. This nonlinear relation of the log I–log V plot can be explained by conduction mechanism based on the Poole–Frenkel (PF) emission. As described PF fitting plot in Fig. 4b, the plot of log I vs. V^{1/2} follows a linear relation. Since amorphous TiO_x has a large number of extrinsic defects [20], the

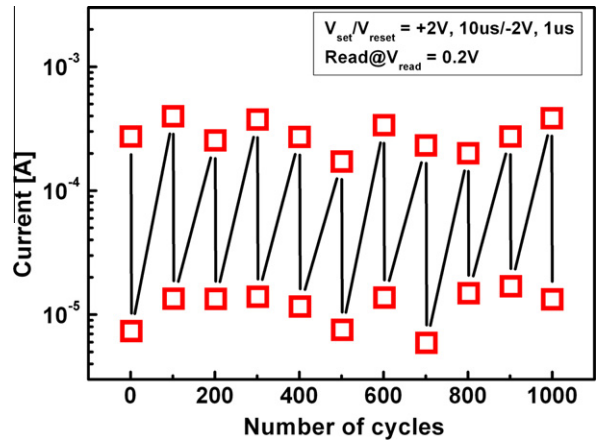


Fig. 6. Cycling endurance characteristics of solution-processed TiO₂-based ReRAM device measured by consecutive ac voltage pulse ($V_{set}/V_{reset} = +2 V, 10 \mu s/-2 V, 1 \mu s$). The current values of HRS/LRS were extracted at $V_{read} = 0.2 V$.

charges can be trapped in these trapping sites and then overcome the energy barrier of the traps at high external bias, which contributes to conduction behavior. This result is consistent with that of a previous result obtained in other amorphous TiO_x-based ReRAM devices [21]. Based on aforementioned analysis, the switching mechanism of our TiO_x-based ReRAM device can be explained by the well-known conductive filament model.

For further analysis, memory reliability was evaluated. The retention characteristic was measured up to high temperature. The excellent temperature dependent stability was confirmed as seen in Fig. 5. There was no noticeable degradation even at 125 °C for 10⁵ s. It is evidently inferred that our TiO_x-based ReRAM device are superior to Al₂O₃- and CuO-based devices, representing unstable retention characteristics at 125 °C [22,23]. The pulse endurance test was also conducted to verify the electrical stability under $V_{set}/V_{reset} = +2 V, 10 \mu s/-2 V, 1 \mu s$ (Fig. 6). Although slight fluctuation was observed, both the resistance states are stable up to 1000th cycles, maintaining resistance difference more than one order of magnitude. All these electrical characteristics indicate that solution-processed TiO_x active layer is obviously suitable for TReRAM application.

Next, the flexibility of solution-processed TiO_x-based ReRAM device was investigated. Fig. 7 shows the comparison of typical I–V curves of ReRAM device formed on flexible PES substrate. To figure out the feasibility for reliable memory switching operation, the I–V measurements were conducted under conditions of

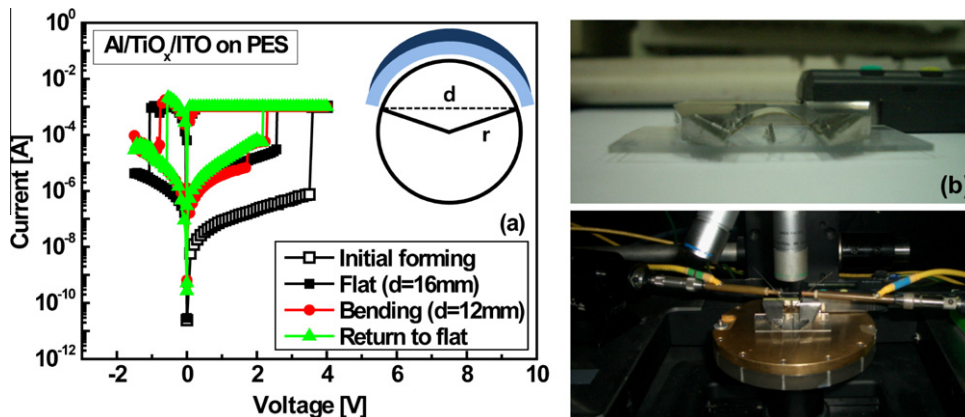


Fig. 7. (a) Typical I–V curves of solution-processed TiO₂-based ReRAM device formed on ITO-coated PES. Bending radius (r) and distance (d) are depicted in the inset of (a). (b) The pictures describing measurement scheme of bent device are also represented.

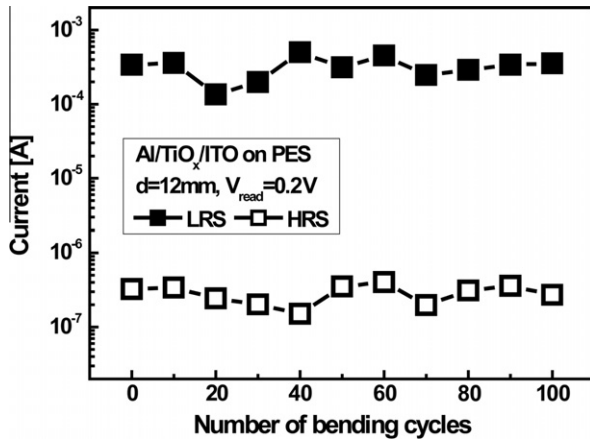


Fig. 8. Current values of HRS/LRS as a function of number of bending cycles. Bending distance was repetitively changed between 16 and 12 mm.

before/during/after bending (Fig. 7a). The evaluation method for bending condition and measurement scheme are depicted in the inset of Fig. 7a and the picture in Fig. 7b, respectively. ‘X mm’ means the minimum distance from one device edge to another. After electrical forming process, even if there is a little instability in current flows, clear resistive switching behaviors were confirmed during and after bending. One of the key requirements for flexible memory application device is the robustness to repetitive bending cycles. In order to verify this characteristic, two resistance states were measured as a function of bending cycles for the device as shown in Fig. 8. During bending endurance measurements, bending distance was consecutively changed between 16 and 12 mm. During 100 bending cycles, no significant changes were observed in both the resistance states. From these results, the feasibility of solution-processed TiO_x-based ReRAM for FRReRAM application was successfully confirmed.

Eventually, nano-scale ReRAM device formed by using solution-processed TiO_x active layer was investigated. Fig. 9a shows typical bipolar switching characteristics under double dc voltage sweep mode, including initial forming, 1st sweep, and 1000th sweep curves. For via-hole device, since the active area of ReRAM device was defined through the size of via-hole, the active area of our device was clearly scaled down to 200 × 200 nm², as seen in Fig. 9b. It should be noted that bipolar switching behavior of solution-processed TiO_x-based ReRAM is still available even in nano-scale regime. Moreover, the stability of resistive switching was preserved during 1000 cycles.

In order to investigate the uniformity of TiO_x-based ReRAM devices with respect to active area, area dependent set/reset voltages

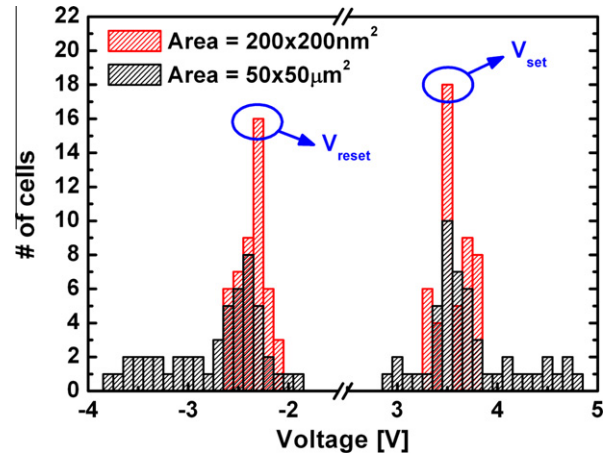


Fig. 10. Uniformity comparison between devices with 50 × 50 μm² and 200 × 200 nm² active area. Set/reset voltages are measured in each 50 fresh devices.

Table 1

Summarized parameters of resistive switching as a function of active area.

Area	2500 μm ²	100 μm ²	25 μm ²	1 μm ²	0.25 μm ²	0.04 μm ²
Parameters						
I _{set} [A]	4.25 E-4	5.1E-4	4.83E-4	6.14E-4	4.18E-4	4.1E-4
I _{reset} [A]	2.67E-6	1.51E-6	1.47E-6	1.18E-6	1.05E-6	7.96E-7
V _{forming} [V]	4.04	4.335	4.375	4.6	4.895	5.095
V _{set} [V]	3.05	3.38	3.395	3.755	4.025	4.255
STDEV (V _{set} /V _{reset})	0.458/0.488	-	-	-	-	0.158/0.136

were monitored in 50 fresh devices, as seen in Fig. 10. Remarkable improvement in switching uniformity was accomplished in the nano-scale device. Other parameters of resistive switching as a function of active area were summarized in Table 1. These uniformity improvement and parameter changes might be attributed to dramatically-reduced number of extrinsic defects due to scale-down of active area, which results in suppressing multi-filament generation [24,25].

In conclusion, we successfully investigated the feasibility of solution-processed TiO_x-based ReRAM devices for transparent, flexible, and nano-scale high-density memory application. Through the combination with ITO-coated glass/PES substrates and nano-scale via-hole structure, our device exhibited stable bipolar

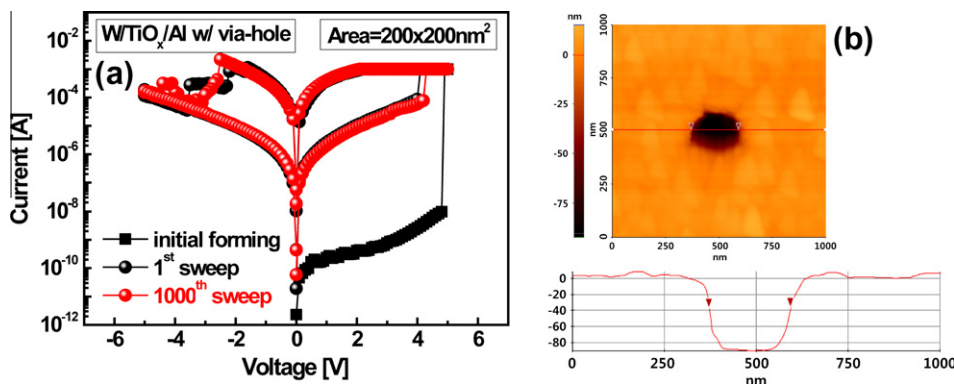


Fig. 9. (a) Typical bipolar switching characteristics of solution-processed TiO₂-based ReRAM device with 200 × 200 nm² active area, including initial forming, 1st, and 1000th sweep. (b) Atomic Force Microscopy image of via-hole structure with 80 nm depth and 200 nm width.

switching behavior and good reliability (endurance and retention characteristics) during maintaining their own unique properties, such as transparency, flexibility, and the feasibility for nano-scale memory.

Acknowledgements

This work was supported by the national research program of the 0.1 Terabit Non-volatile Memory Development Project and the National Research Laboratory (NRL) Programs of the Korea Science and Engineering Foundation (KOSEF).

References

- [1] International Technology Roadmap for Semiconductors (ITRS) 2010.
- [2] R. Waser, M. Aono, *Nat. Mater.* 6 (2007) 833.
- [3] J. Yang, M. Pickett, X. Li, D. Ohlberg, D. Stewart, R. Williams, *Nat. Nanotechnol.* 3 (2008) 429.
- [4] D. Kwon, K. Kim, J. Jang, J. Jeon, M. Lee, G. Kim, X. Li, G. Park, B. Lee, S. Han, M. Kim, C. Hwang, *Nat. Nanotechnol.* 5 (2010) 148.
- [5] A. Beck, J.G. Bednorz, Ch. Gerber, C. Rossel, D. Widmer, *Appl. Phys. Lett.* 77 (2000) 139.
- [6] D. Seong, M. Jo, D. Lee, H. Hwang, *Electrochem. Solid-State Lett.* 10 (2007) H168.
- [7] A. Sawa, T. Fujii, M. Kawasaki, Y. Tokura, *Appl. Phys. Lett.* 88 (2006) 232112.
- [8] D. Seong, J. Park, N. Lee, M. Hasan, S. Jung, H. Choi, J. Lee, M. Jo, W. Lee, S. Park, S. Kim, Y. Jang, Y. Lee, M. Sung, D. Kil, Y. Hwang, S. Chung, S. Hong, J. Roh, H. Hwang, *IEDM Tech Digest.* (2009) 101.
- [9] N. Gergel-Hackett, B. Hamadani, B. Dunlap, J. Suehle, C. Richter, C. Hacker, D. Gundlach, *IEEE Electron Device Lett.* 30 (2009) 706.
- [10] J. Yun, K. Cho, B. Park, B. Park, S. Kim, *J. Mater. Chem.* 19 (2009) 2082.
- [11] C. Lee, I. Kim, W. Choi, H. Shin, J. Cho, *Langmuir* 25 (2009) 4274.
- [12] S. Kim, H. Moon, D. Gupta, S. Yoo, Y. Choi, *IEEE Trans. Electron Devices* 56 (2009) 696.
- [13] J. Kim, S. Kim, H. Lee, K. Lee, W. Ma, X. Gong, A. Heeger, *Adv. Mater.* 18 (2006) 572.
- [14] S. Cho, K. Lee, A.J. Heeger, *Adv. Mater.* 21 (2009) 1941.
- [15] C.D. Wagner, A.V. Naumkin, A. Kraut-Vass, J.W. Allison, C.J. Powell, J.R. Rumble, NIST X-ray Photoelectron Spectroscopy Database, version 3.5 (Web version), National Institute of Standards and Technology, Gaithersburg, MD, 2003.
- [16] S. Jung, J. Kong, S. Song, K. Lee, T. Lee, H. Hwang, S. Jeon, *J. Electrochem. Soc.* 157 (2010) H1042.
- [17] I. Kim, S. Jung, J. Shin, K. Biju, K. Seo, M. Siddik, X. Liu, J. Kong, K. Lee, H. Hwang, *Jpn. J. Appl. Phys.* 50 (2011) 046504.
- [18] C. Rohde, B. Choi, D. Jeong, S. Choi, J. Zhao, C. Hwang, *Appl. Phys. Lett.* 86 (2005) 262907.
- [19] D. Jeong, H. Schroeder, R. Waser, *Appl. Phys. Lett.* 89 (2006) 082909.
- [20] C. Chang, S.M. Sze, *ULSI Technology*, McGraw-Hill International, 1996, p. 178.
- [21] H. Jeong, J. Lee, M. Ryu, S. Choi, *Phys Status Solidi-R.* 4 (2010) 28.
- [22] S. Kim, Y. Choi, *Appl. Phys. Lett.* 92 (2008) 223508.
- [23] H.B. Lv, M. Yin, X.F. Fu, Y.L. Song, L. Tang, P. Zhou, C.H. Zhao, T.A. Tang, B.A. Chen, Y.Y. Lin, *IEEE Electron Device Lett.* 29 (2008) 309.
- [24] J. Lee, J. Shin, D. Lee, W. Lee, S. Jung, M. Jo, J. Park, K. Biju, S. Kim, S. Park, H. Hwang, *IEDM Tech Digest.* (2010) 452.
- [25] T. Kim, H. Choi, S. Oh, M. Jo, G. Wang, B. Cho, D. Kim, H. Hwang, T. Lee, *Nanotechnology* 20 (2009) 025201.